Verified and validated finite element analyses of humeri

Gal Dahan[a], Nir Trabelsi[b], Ori Safran[c], Zohar Yosibash[a,*]

[a]*Department of Mechanical Engineering, Ben-Gurion University, Beer-Sheva, Israel*
[b]*Department of Mechanical Engineering, Shamoon College of Engineering, Beer-Sheva, Israel*
[c]*Department of Orthopaedics, Hadassah University Hospital, Jerusalem, Israel*

Abstract

Background: Although ∼200,000 emergency room visits per year in the US alone are associated with fractures of the proximal humerus, only limited studies exist on their mechanical response. We hypothesise that for the proximal humeri a) the mechanical response can be well predicted by using inhomogeneous isotropic material properties, b) the relation between bone elastic modulus and ash density ($E(\rho_{ash})$) is similar for the humerus and the femur, and may be general for long bones , and c) it is possible to replicate a proximal humerus fracture in-vitro by applying uniaxial compression on humerus' head at a prescribed angle.

Methods: Four fresh frozen proximal humeri were CT-scanned, instrumented by strain-gauges and loaded at three inclination angles. Thereafter head displacement was applied to obtain a fracture. CT-based high order (p-) finite element (FE) and classical (h-) FE analyses were performed that mimic the experiments and predicted strains were compared to the experimental observations.

Results: The $E(\rho_{ash})$ relationship appropriate for the femur, is equally appropriate for the humeri: predicted strains in the elastic range showed an excellent agreement with experimental observations with a linear regression slope of $m = 1.09$ and a coefficient of regression $R^2 = 0.98$. $p-$FE and h-FE results were similar for the linear elastic response. Although fractures of the proximal humeri were realized in the in-vitro experiments, the contact FE analyses (FEA) were unsuccessful in representing properly the experimental boundary conditions.

*Corresponding author
Email address: `zohary@bgu.ac.il` (Zohar Yosibash)

Discussion: The three hypotheses were confirmed and the linear elastic response of the proximal humerus, attributed to stage at which the cortex bone is intact, was well predicted by the FEA. Due to a large post-elastic behavior following the cortex fracture, a new non-linear constitutive model for proximal humerus needs to be incorporated into the FEA to well represent proximal humerus fractures. Thereafter, more in-vitro experiments are to be performed, under boundary conditions that may be well represented by the FEA, to allow a reliable simulation of the fracture process.

---

1. Introduction

Proximal humerus fractures are common, accounting for 4% to 5% of all fractures in the elderly, with a 7:3 female to male ratio (Court-Brown et al., 2001; Kim et al., 2012). Proximal humerus fractures are the third most common osteoporotic fractures after the femur and the distal radius, with almost 200,000 emergency room visits that occurred in 2008 in the US alone (Kim et al., 2012). One of the common fracture types is a fracture of the proximal humerus, an outcome of falling on an out-stretched arm that may occur during daily activities. Although 80% of shoulder fractures may be treated conservatively (Petit et al., 2009), a wide variety of surgical options are being applied with no quantitative tool available to assist the surgeon to decide whether to operate or not, and if operation is necessary what is the optimal operational strategy.

Despite this necessity, no verified and validated simulations of humeri are available, nor are loading conditions or experimental observations that result in proximal humerus fractures.In (Maldonado et al., 2003), FEA of two humeri under muscles physiological-like loading was presented, in addition to simple compression and torsion tests. Validation by in-vitro experiments was made only for the simple non-physiological loading cases and by means of only two values of stiffness. Finite element models representing physiological loads were also presented in (Clavert et al., 2006), but these were not validated by experiments. In (Varghese et al., 2011), three point bending and torsion experiments were conducted on ten humeri shafts. Only for one humerus a FE analysis was performed that did not mimic a physiologic load.

Regarding the physiological loads on the humerus during daily activities, and specifically for "falling on an out-stretched arm", these are determined mostly by biomechanical models applying muscle forces (Karlsson and Peterson, 1992; Dul, 1988; van der Helm, 1994), measurements in-vivo (Bergmann et al., 2011, 2007; Westerhoff et al., 2009) or kinetics and kinematics equations while measuring ground reaction force (Hsu et al., 2011; Chou et al., 2001). Table 1 summarizes the magnitude and directions of loads reported. All configurations refer to the coordinate system in which the X-axis points anteriorly, Y axially to connect the humeral head and elbow center (between the medial and lateral epycondyles), and Z laterally in a plane spanned by the elbow axis and Y-axis (see Figure 1).

[Figure 1 about here.]

[Table 1 about here.]

Inspecting Table 1, one may conclude that during daily life activities the loads on the humerus act at $\alpha \sim 35°$. During falling on out-stretched arm, one may notice that the loads magnitude calculated by (Hsu et al., 2011; Chou et al., 2001) are lower than those measured during daily life activities (Bergmann et al., 2011, 2007; Westerhoff et al., 2009). Aside from the fact that the loads reported in (Hsu et al., 2011; Chou et al., 2001) were not measured in-vivo, the subjects performed forward falling from low height (to avoid risk of injury) which resulted in both lower force magnitudes and different upper arm orientations than expected in an actual fall.

High order personalized finite element analyses (p-FEAs) based on quantitative computed tomography (QCT) were shown to predict well the mechanical response when compared to in-vitro experiments for intact and implanted femurs, femurs with metastatic tumors and even metatarsal bones (Yosibash et al., 2007a,b; Trabelsi et al., 2009, 2011, 2014; Yosibash et al., 2014). p-FEAs have many advantages over classical FEAs named h-FEAs: the p-FE mesh is unchanged and convergence of the results is considerably faster as the polynomial degree is increased in the background, the p-elements may be much larger and by far more distorted, the numerical error of the p-FE solution is well estimated and provided, and the bone's surfaces is accurately represented by smooth surfaces. Using similar p-FEAs we hypothesise that for the proximal humeri a) the mechanical response can be well predicted by using inhomogeneous isotropic material properties, b) the relation between bone elastic modulus and ash density ($E(\rho_{ash})$) is general for long bones, and c) it is possible to replicate a proximal humerus fracture in-vitro by applying uniaxial compression at a prescribed angle. The specific goals are to determine whether the techniques of assigning mechanical properties to p-FEA (based on CT scans) to femurs are equally well applied to humeri, to validate the p-FEA results by experiments that simulate physiological-like loads on fresh frozen humeri, and finally to present an experimental system that imposes on a fresh-frozen humerus loading conditions that simulate fractures noticed while "falling on an out-stretched arm". In this study we also perform contact analyses using h-FEA. To evaluate its prediction capabilities we compare p-FEA results to classical (h-FEA) results for a well defined linear analysis.

2. Materials and Methods

Four human humeri (2 pairs, denoted by FFH1 and FFH2) were frozen shortly after death, and were kept at $-80°C$ until the experiment. Donors details are:

Donor Label	Age (Years)	Height [m]	Weight [Kg]	Gender
FFH1	68	1.62	125	Female
FFH2	51	1.75	77	Female

The humeri were cleaned from soft tissues and degreased with ethanol, cut approximately 260 mm from the top (100 mm below the deltoid tuberosity) and its distal end was fixed into a cylindrical metallic sleeve by PMMA, positioned according the coordinate system suggested by (Wu et al., 2005), *i.e.* the two epicondyles of the elbow joint are aligned with the humeral head center in one plane. The humeri were immersed in water and scanned with K_2HPO_4 calibration phantoms using a Philips Brilliance 64 CT scanner (Einhoven, Netherlands - 120 kVp, 250 mAs, 1.25 mm slice thickness). Axial scan without overlap and pixel size of 0.2

mm were used. Ten to twelve uniaxial Vishay C2A-06-125LW-350 strain gauges (SG) were bonded to the surface, positioned along the expected principal directions. The SGs locations and general geometrical sizes were taken using a caliber and by photographs, see Figure 2 for typical SG location.

2.1. In-vitro experiments

Experiments were conducted on each pair (right and left) at the same day of defrosting. A uniaxial force was applied at three different angles to the humeri heads. To represent physiological loads during daily activities the force was applied at $\alpha = 35°$ with an inclination $\beta = 20°$ also in XY plane (Bergmann et al., 2011). To represent a proximal humerus fracture,two different loads were considered: the original ZY plane (denoted by scapular plane, in which the scapula and humerus are located anatomically) was rotated by 24° along the Y axis, and in this new plane loads at 15° and 20° were applied, see Fig. 1 bottom.

The load was applied to the femur by a spherical-shaped cup (Figure 2 (b)) made of PMMA which constrained the movement of the humeri perpendicular to the applied load direction, thus resulting in forces on the humerus head also perpendicular to the applied load. The distal part of the humeri was clamped in the metallic cylindrical sleeve.

To allow a precise representation of the boundary conditions for the FE analyses in the elastic range, two of the humeri (FFH2 right and left) were additionally loaded by a flat low friction plate (Figure 2 (a)). A fracture at the proximal humerus cannot be obtained by the flat plate loading because of the resulting lateral movement of the head that causes high stresses at the clamped distal end (fracture would had been obtained at the clamped distal end).

[Figure 2 about here.]

Load was applied by a Shimadzu AG-IC machine (Shimadzu Corporation, Kyoto, Japan) with a load cell of 20kN (precision of $\pm 0.5\%$). Strains, axial force and displacements (horizontal, vertical and vertical to the bone's shaft) of the head were recorded by a Vishay 7000 data-logger. To confirm repeatability, each load was repeated two to five times (loads of 300 to 600 N were applied). Loading rate was 5 $\frac{mm}{min}$ while strains and displacements were recorded at a sampling rate of 128 Hz. To examine bone's linear elastic response, the results for each SG at each loading and inclination with the corresponding linear regressions were plotted and analyzed. The average slope of each SG at each angle was calculated and multiplied by 800 [N] for comparison with the FE results. The same procedure was performed for the recorded displacements. Following the compression experiments, vertical displacement was applied to the humeri using the spherical shaped cup at the 20° configuration, at a rate of 10 $\frac{mm}{min}$ until fracture of the head was observed. The fracture experiment data was recorded at a sampling rate of 512 Hz.

2.2. FE analyses

FE linear elastic analyses mimicking the experimental flat loading configuration of FFH2 humeri were performed using both high order finite elements (p-FE) and the classical h-FE (Abaqus[1]). To model the spherical shaped cup experiments, contact analyses were performed using Abaqus. The QCT-based p-FE models were semi-automatically constructed following the methods detailed in (Yosibash et al., 2007a,b) and illustrated in Figure 3. A tetrahedral mesh was created ($\sim$ 2500 elements, avg. length 10 mm) and refined at areas of interest.

The h-FE model construction and material properties assignment is described herein. Second order tetrahedral elements (between 60,000 to 200,000, avg. length 2 mm)) were generated automatically. For each model, a file containing the nodes coordinates was exported from Abaqus and imported to a semi-automated Matlab code assigning to each node a value of Young's modulus from the closest point found in the CT data. Using this file, a nodal-wise temperature field was defined in the model. To assign the heterogenous material properties, a temperature dependent material was defined by setting the Young modulus to be equal to the temperature at each node, i.e. 10 different material properties per each tetrahedral element.

[Figure 3 about here.]

[1]Abaqus is a trademark of Dassault Systèmes Simulia Corp., Providence, RI, USA.

2.2.1. Material properties

For axial loading conditions an inhomogeneous isotropic material assignment to FE models well represents the bone's mechanical response (Yosibash et al., 2007b; Schileo et al., 2007; Yosibash et al., 2014). K_2HPO_4 liquid phantoms were scanned with the humeri while immersed in water, obtaining the following relations:

$$\begin{aligned} FFH1: \rho_{K_2HPO_4}\ [gr/cm^3] &= 10^{-3} \cdot (0.816 \cdot HU + 6) \\ FFH2: \rho_{K_2HPO_4}\ [gr/cm^3] &= 10^{-3} \cdot (0.807 \cdot HU - 1.6) \end{aligned} \tag{1}$$

Converting $\rho_{K_2HPO_4}$ to ash density ρ_{ash} was performed based on (Schileo et al., 2008) and a relation between hydroxyapatite and K_2HPO_4 phantoms given in (M.M, 1992):

$$\rho_{ash}\ [gr/cm^3] = 0.877 \times 1.21 \times \rho_{K_2HPO_4} + 0.08 \tag{2}$$

FE models using the $E(\rho_{ash})$ relations documented in (Keyak et al., 1993) and (Keller, 1994) were shown to provide excellent results when comparing to *in-vitro* experiments (see also (Yosibash et al., 2014)):

$$E_{cort} = 10200 \cdot \rho_{ash}^{2.01}\ [MPa], \quad \rho_{ash} \geq 0.486\ [gr/cm^3] \tag{3}$$

$$E_{trab} = 2398\ [MPa], \quad 0.3 < \rho_{ash} < 0.486\ [gr/cm^3] \tag{4}$$

$$E_{trab} = 33900 \cdot \rho_{ash}^{2.2}\ [MPa], \quad \rho_{ash} \leq 0.3\ [gr/cm^3] \tag{5}$$

The relation reported in (Keller, 1994) includes specimens with a wide density range ($0.092 < \rho_{ash} < 1.22\ [g/cm^3]$) while the relation reported in (Keyak et al., 1993) was obtained using lower ash densities $< 0.3\ [g/cm^3]$. Since no exact HU value that distinguishes between cortical and trabecular bone regions exists, based on the experience gained in previous work on the *femur*, $HU > 475$ was associated with cortical bone. This threshold value leads to different values of Young's modulus when substituting in (3) and (5). Therefore for any $\rho_{ash} < 0.3 g/cm^3$, E was determined using (5) and a constant value of 2398 MPa was used in the gap created between the two densities.

2.2.2. Boundary conditions and post-processing of FE results

FE models were fully constrained at the distal part of the shaft and a compression force of 800 N was applied on a planar circular area (1 cm diameter) at the top of the humeri head at the respective angles (15°, 20° and 35° + 20°) (see top of Fig. 4).

[Figure 4 about here.]

The p-FE models were solved by increasing the polynomial degree while monitoring the convergence in energy norm. In case of poor local convergence, a local refinement and a new analysis were performed. In addition h-FE linear and contact analyses to simulate the flat load were performed. For the contact analyses, normal displacement was applied to a flat plate above the humerus head until a reaction force of 800 N was obtained. Mesh refinement was performed until convergence in local values of interest was obtained.

To mimic the experiments performed with the spherical shaped cup, contact analyses were performed using Abaqus. A CAD model of the spherical shaped cup was imported into Abaqus and positioned above the bone's model to mimic the experimental configuration. A normal displacement was applied to its upper surface until the desired reaction force measured in the experiment was obtained.

The average strain was extracted from FE results along pre-determined curves indicating the SGs locations, whereas displacements were extracted at nodes. Since uni-axial SGs were used in all experiments, the FE strain component was considered in the direction coinciding with the SG direction, usually aligned along the local principal strain directions (E_1 or E_3). If the SG was found not to align with the principal strain, a local system was positioned and the strain value was extracted in the new system.

p-FEMs were proven in former studies to accurately predict the mechanical response of bones (Yosibash et al., 2007b; Trabelsi et al., 2011, 2014; Yosibash et al., 2014). Contact algorithms are unavailable in the p-FE solver thus for contact analyses the h-FE solver Abaqus was used. To evaluate the accuracy of Abaqus results, a comparison between the FE results from both solvers was made for the models loaded by the flat plate.

The predictability of the finite element analyses was examined by comparing the FEA results with the experimental observations. Statistical analysis is based on a standard linear regression, where a perfect correlation is evident by a unit slope, a zero intercept and a unit R^2 (linear correlation coefficient). The results are shown also in a Bland-Altman error plot $((EXP-FE), \frac{EXP-FE}{2})$. The mean error, absolute mean error and root mean square error (RMSE) were also calculated:

$$\text{Mean Error} = \frac{100}{N}\Sigma_{i=1}^{N}\frac{(Exp_{(i)}-FE_{(i)})}{Exp_{(i)}} \quad [\%] \tag{6}$$

$$\text{Mean absolute Error} = \frac{100}{N}\Sigma_{i=1}^{N}\left|\frac{(Exp_{(i)}-FE_{(i)})}{Exp_{(i)}}\right| \quad [\%] \tag{7}$$

$$\text{RMSE} = \sqrt{\frac{1}{N}\Sigma_{i=1}^{N}(Exp_{(i)}-FE_{(i)})^2} \tag{8}$$

3. Results

3.1. Experimental observations

Strains and displacements recorded during the experiments with the flat punch (excluding the experiment to fracture) showed a linear relationship with the applied load applied until 800N.

Force-strain response at SGs close to fracture location in the experiments to fracture (20^o inclination with the spherical shaped cup) becomes non-linear, as expected, as the applied displacement on the humerus head increases. Fracture locations (pointed by white arrows) and the applied force vs. largest measured strain are presented in Fig. 5.

[Figure 5 about here.]

3.2. *FE results compared to experimental observations*

All FE models of FFH2 humeri loaded by a flat plate converged to less than 6% relative error in energy norm at $p = 8$. For example, the principal strain ϵ_3 at $800N$ for one of the humeri at three loading inclinations is presented in Fig. 4. Because the FE models were clamped, smaller FE displacements (by a factor of about 2) were obtained compared to measured displacements. This is because the part of the bone imbedded in PMMA, and the jig it was fixed to, underwent elastic displacements. Thus FE displacements were not compared to the measured ones. Linear regression and Bland-Altman plots for FFH2 humeri loaded by a flat plate are presented in Fig. 6. The mean error (6), mean absolute error (7) and the root mean square error (8) are:

	FFH2L			FFH2R		
Inclination	Mean Error [%]	Absolute Mean Error [%]	RMSE [$\mu strain$]	Mean Error [%]	Absolute Mean Error [%]	RMSE [$\mu strain$]
15°	-3.9	9.2	127	-6.7	17.3	270.7
20°	-5.6	16.2	166	-12.7	21.9	393.3
35°	-6.2	16.5	453	-5	18.2	678.1
Total	-5.2	13.9	278.5	-8.3	19.1	471.9

[Figure 6 about here.]

Contact analyses performed to mimic the fracture experiments were not comparable to experimental observations. As shown in Fig. 7 the computed contact area on the humeral heads did not correspond to these in experiments. Therefore, the direction and location of the applied load on the humeri in the experiments cannot be determined by a contact FE analysis performed. Thus we cannot compare the predicted strains at fracture with the experimental observations.

[Figure 7 about here.]

3.3. *p-FEA vs h-FEA*

To evaluate the accuracy of classical h-FEAs compared to p-FEAs, three flat loading configurations of one humerus (FFH2L) were also computed by linear elastic analyses in Abaqus. The h-FE mesh consisting of

209953 second order tetrahedral elements and 902037 DOF compared to the p-FE mesh containing 2767 elements and 758280 DOF are shown in Figure 4. The model that represents FFH2L loaded at 35° by a flat plate was also solved by a contact analysis considering the frictionless contact between the plate and the humerus. An excellent linear correlations between h and p linear analyses for FFH2L was obtained with a slope of 0.987 and $R^2 = 0.994$.

4. Discussion

The ability to compute the strength and stiffness of humeri can serve as a valuable tool for an orthopedic surgeon for diagnosis and treatment desicions. The necessity of surgical intervention and type of intervention could be determined using quantitative predictions rather than educated assessments, X-ray examinations or surgeon's experience. The use of CT-based patient specific FEA to predict bones' mechanical response is extensively examined in the last decade, mostly on femurs (Schileo et al., 2007; Trabelsi et al., 2009, 2011; Yosibash et al., 2014). This study is aimed at investigating whether the methods validated for femurs may be applied to predict the mechanical response of the proximal humeri.

$E(\rho_{ash})$ relationship (3)-(5) derived for femurs and used in FEAs of femurs (Yosibash and Trabelsi, 2012; Yosibash et al., 2014) were shown to well predict the linear elastic response of humeri. The predicted strains showed an excellent correlation with the experimental measurements (based on two specimens), with a linear regression slope of $m = 1.09$ and a correlation coefficient $R^2 = 0.98$. For comparison, for 17 femurs using similar $E(\rho_{ash})$ relations $m = 0.961$ and $R^2 = 0.965$ were obtained (Yosibash and Trabelsi, 2012). An example of the predicted principal compression strains in the humerus (at 15^o loading) and the distribution of the ash density is shown in Fig. 8.

[Figure 8 about here.]

Unlike in femurs, the humerus head has a much thinner outer cortical shell. We observed that the trabecular zone of the humeri we scanned had a very low Young modulus which is mostly homogenous distributed. This suggests that the fracture may be mostly affected by strains in the cortex due to the change of curvature in the head-shaft intersection.

Classical h-FEA was compared to p-FEA for one humerus at three loading inclinations. p-FEAs have a major advantage over h-FEA because the error in the numerical results is intrinsically obtained and is much more efficient. For example, to obtain 10% relative error in energy norm, $\sim 150,000$ DOF were required for the h-FE model compared to $\sim 50,000$ for the p-FE model. It is also important to realize that local data of interest as the strains converge much faster and more monotonically using p-FEMs compared to h-FEMs as clearly shown in Fig. 9. Although at the "end of the day", both h- and p-FE methods match closely if the number of DOF is high enough, p-FEMs allow intrinsic quantification of numerical errors which h-FEMs do not. h-FE analyses of humeri presented in (Maldonado et al., 2003; Clavert et al., 2006; Varghese et al., 2011) do not present any verification of the numerical results. In (Maldonado et al., 2003) the proximal humeri FE mesh contained about 150,000 DOF and in (Clavert et al., 2006) the proximal third of the humerus was meshed with more than 200,000 elements but none report verification of the numerical results.

[Figure 9 about here.]

An in-vitro experimental configuration that may induce proximal humeri fractures was demonstrated. Up to $-5000\mu strain$ were measured at fracture's surface (Fig. 5). Since the fracture-experiments are displacement controlled, one can identify a large range of post-elastic (nonlinear) behavior, especially for FFH1L. To the best of our knowledge this is the first published set of experiments that replicate in-vitro fractures of the proximal humerus.

Attempting to apply contact boundary conditions in the FEA to replicate the sphere-shaped cup loading showed a high sensitivity of the results to small variations in the applied load location and direction (determined by the contact analysis). Furthermore, the contact analysis resulted in a force direction and location which does not coincide with these observed in the experiments. The reasons for this discrepancy can be: a) Insufficient accuracy of the geometry of the humerus FE model constructed from the CT-scan (which is necessary when addressing contact between two surfaces). b) The thin layer of cartilage covering the humeral head that may incorrectly represent the exact location where the load is being applied. c) Lack of a post-elastic constitutive model that may dramatically change the FE predicted mechanical response compared to the linear elastic response. In an attempt to allow a reliable simulation of the post-elastic response of the proximal humerus that well represents the fracture etiology (postulated to occur once the cortex fractures) a new constitutive model must be developed and a new experimental system should be designed that will allow a precise determination of the applied force.

There are several limitations to the present study: a) The applicability of inhomogeneous isotropic material properties was investigated for a simplified compression boundary condition. A more complex loading may require more realistic orthotropic material properties (as the orthotropic properties given in (Grande-Garcia, 2012)). b) The distal part of the bone embedded in PMMA constrained by a metallic cylinder was modeled as fixed. This simplification resulted in poor agreement between measured and computed displacements. c) The physiological loads excerted on the proximal humerus by the muscles during a fracture are unavailable, and were assumed to be negligible compared to the uniaxial compression load applied by the scapula on humerus' head.

We conclude that: a) The linear elastic response of the proximal humerus can be predicted by FEA using inhomogeneous isotropic material properties, b) The relation between bone elastic modulus and ash density ($E(\rho_{ash})$) is similar for the humerus and the femur for the elastic regime, and c) Proximal humerus fractures can be replicated in-vitro by applying uniaxial compression on humerus' head, showing a large post-elastic behaivor following the cortex fracture, thus possibly a new non-linear constitutive model for proximal humeurs needs to be incorporated into the FEA.

Conflict of Interest

None of the authors have any conflict of interest to declare that could bias the presented work.

Acknowledgements

The authors thank Prof. Charles Milgrom, from the Hadassah Hospital for helpful discussions and Mr. Ilan Gilad and Yekutiel Katz, from the Ben Gurion University for their assistance with the experiments. This study was made possible through the generous support of a (*Milgrom Foundation for Science*) grant.

References

Bergmann, G., Graichen, F., Bender, A., Kääb, M., Rohlmann, A., Westerhoff, P., 2007. In vivo glenohumeral contact forces - Measurements in the first patient 7 months postoperatively. Jour. Biomech. 40, 2139–2149.

Bergmann, G., Graichen, F., Bender, A., Rohlmann, A., Halder, A., Beier, A., Westerhoff, P., 2011. In vivo gleno-humeral joint loads during forward flexion and abduction. Jour. Biomech. 44, 1543–1552.

Chou, P., Chou, Y., Lin, C., Su, F., Lou, S., Lin, C., Huang, G., 2001. Effect of elbow flexionon upper extremity impact forces during a fall. Clin. Biomech. 16, 888–894.

Clavert, P., Zerah, M., Krier, J., Mille, P., Kempf, J., Kahn, J., 2006. Finite element analysis of the strain distribution in the humeral head tubercles during abduction: comparison of young and osteoporotic bone. Surgical and Radiologic Anatomy 28, 581–587.

Court-Brown, C., Garg, A., McQueen, M., 2001. The epidemiology of proximal humeral fractures. Acta Orthopaedica Scandinavica 72, 365–371.

Dul, J., 1988. A biomechanical model to quantify shoulder load at the work place. Clin. Biomech. 3, 124–128.

Grande-Garcia, E., 2012. Double experimental procedure for model-specific finite element analysis of the human femur and trabecular bone. Ph.D. thesis. Technical Univ. of Munich. Munich, Germany. Https://mediatum.ub.tum.de/doc/1118982/1118982.pdf.

van der Helm, F., 1994. Analysis of the kinematic and dynamic behavior of the shoulder mechannism. Jour. Biomech. 27, 527–550.

Hsu, H., Chou, Y., Lou, S., Huang, M., Chou, P., 2011. Effect of forearm axially rotated posture on shoulder load and shoulder abduction / flexion angles in one-armed arrest of forward falls. Clin. Biomech. 26, 245–249.

Karlsson, D., Peterson, B., 1992. Towards a model for force predictions in the human shoulder. Jour. Biomech. 25, 189–199.

Keller, T.S., 1994. Predicting the compressive mechanical behavior of bone. Jour. Biomech. 27, 1159–1168.

Keyak, J.., Fourkas, M.G., Meagher, J.M., Skinner, H.B., 1993. Validation of automated method of three-dimensional finite element modelling of bone. ASME Jour. Biomech. Eng. 15, 505–509.

Kim, S., Szabo, R., Marder, R., 2012. Epidemiology of humerus fractures in the united states: Nationwide emergency department sample, 2008. Arthritis Care & Research 64, 407–414.

Maldonado, Z., Seebeck, J., Heller, M., Brandt, D., Hepp, P., Lill, H., Duda, G., 2003. Straining of the intact and fractured proximal humerus under physiological-like loading. Jour. Biomech. 36, 1865–1873.

M.M, G., 1992. Conversion relations for quantitative ct bone mineral densities measured with solid and liquid calibration standards. Bone. and. Mineral 19, 145–158.

Petit, C., Millett, P., Endres, N., Diller, D., Harris, M., Warner, J., 2009. Management of proximal humeral fractures: Surgeons don't agree. Journal of shoulder and elbow surgery 19, 446–451.

Schileo, E., DallAra, E., Taddei, F., Malandrino, A., Schotkamp, T., Baleani, M., Viceconti, M., 2008. An accurate estimation of bone density improves the accuracy of subject-specific finite element models. Jour. Biomech. 41, 2483–2491.

Schileo, E., Taddei, F., Malandrino, A., Cristofolini, L., Viceconti, M., 2007. Subject-specific finite element models can accurately predict strain levels in long bones. Jour. Biomech. 40, 2982–2989.

Trabelsi, N., Milgrom, C., Yosibash, Z., 2014. Patient-specific fe analyses of metatarsal bones with inhomogeneous isotropic material properties. Journal of the mechanical behavior of biomedical materials 29, 177–189.

Trabelsi, N., Yosibash, Z., Milgrom, C., 2009. Validation of subject-specific automated p-FE analysis of the proximal femur. Jour. Biomech. 42, 234–241.

Trabelsi, N., Yosibash, Z., Wutte, C., Augat, P., Eberle, S., 2011. Patient-specific finite element analysis of the human femur - a double-blinded biomechanical validation. Jour. Biomech. 44, 1666 – 1672.

Varghese, B., Short, D., Penmetsa, R., Goswami, T., Hangartner, T., 2011. Computed-tomography-based finite-element models of long bones can accurately capture strain response to bending and torsion. Jour. Biomech. 44, 1374 – 1379.

Westerhoff, P., Graichen, F., Bender, A., Halder, A., Beier, A., Rohlmann, A., Bergmann, G., 2009. In vivo measurement of shoulder joint loads during activities of daily living. Jour. Biomech. 42, 1840–1849.

Wu, G., van der Helm, F., Veegerc, H., Makhsouse, M., Van Roy, P., Anglin, C., Nagels, J., Karduna, A.R.and McQuade, K., Wang, X., Werner, F., Buchholz, B., 2005. ISB recommendation on definitions of joint coordinate systems of various joints for the reporting of human joint motion - Part II: shoulder, elbow, wrist and hand. Jour. Biomech. 38, 981–992.

Yosibash, Z., Padan, R., Joscowicz, L., Milgrom, C., 2007a. A CT-based high-order finite element analysis of the human proximal femur compared to in-vitro experiments. ASME Jour. Biomech. Eng. 129, 297–309.

Yosibash, Z., Plitman Mayo, R., Dahan, G., Trabelsi, N., Amir, G., Milgrom, C., 2014. Predicting the stiffness and strength of human femurs with realistic metastatic tumors. Bone 69, 180–190.

Yosibash, Z., Trabelsi, N., 2012. Reliable patient-specific simulations of the femur, in: A., G. (Ed.), Patient-Specific Modeling in Tomorrow's Medicine. Springer, pp. 3–26.

Yosibash, Z., Trabelsi, N., Milgrom, C., 2007b. Reliable simulations of the human proximal femur by high-order finite element analysis validated by experimental observations. Jour. Biomech. 40, 3688–3699.

Tables

Table 1: Summary of humerus loads as found in the literature

Reference	Method	Task	Force magnitude		Force direction	
			N	%BW	α	β
Van der-Helm (1994)	3-D biomechanical model	90^o flexion	182	-	-	-
		90^o abduction	458	-	-	-
Dul (1988)	2-D biomechanical model	87^o abduction	-	43	-	-
Karlsson & Peterson (1992)	3-D biomechanical model	60^o abduction	650	-	-	-
Bergmann et al. (2007)	in-vivo measurement (Shoulder implant)	90^o flexion (no weight)	764	78	-	-
		90^o flexion (2 Kg in hand)	1254	128	14^o	26^o
Bergmann et al. (2011)	in-vivo measurement (Shoulder implant)	90^o flexion (2 Kg in hand)	1050	120	32^o	19^o
		90^o abduction (2 Kg in hand)	1125	132	29^o	23^o
Westerhoff et al. (2009)	in-vivo measurement (Shoulder implant)	Different daily activities	560-980	75-130	-	-
Chou et al. (2001)	Calculations using GRF	FOOSA-extented elbow	303	44.6	12^o	28^o
		FOOSA-flexed elbow	377	55.5	17^o	38^o
Hsu et al. (2011)	Calculations using GRF	FOOSA	423	59	15^o	22^o

GRF-Ground reaction force. FOOSA-Fall on out-stretched arm.
α- angle of the force in YZ plane. β- angle of the force in XY plane.

Figures

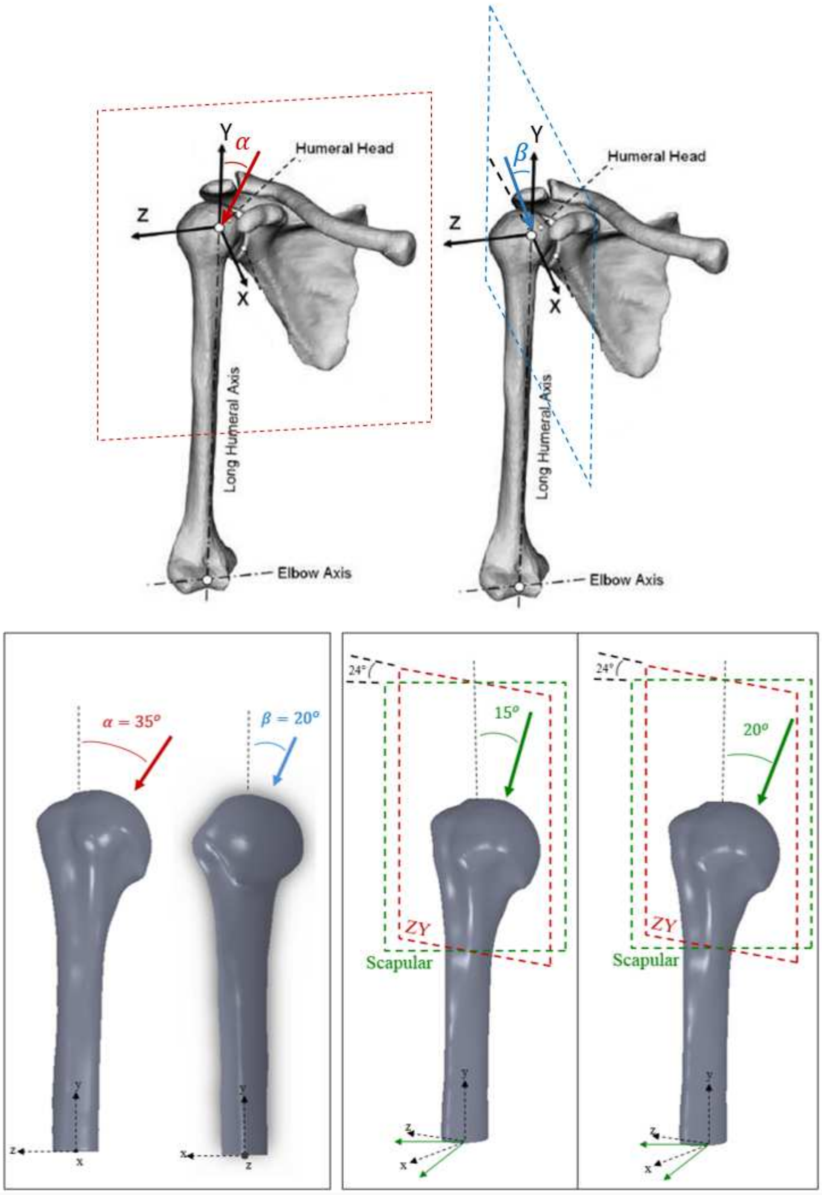

Figure 1: Top: Humerus coordinate system as suggested by (Wu et al., 2005), α is the angle in YZ plane, β is the angle in XY plane. Bottom: Experimental loads on the proximal humerus. At $\alpha = 35°, \beta = 20°$ and at 15° and 20° inclinations (loads acting in the scapular plane).

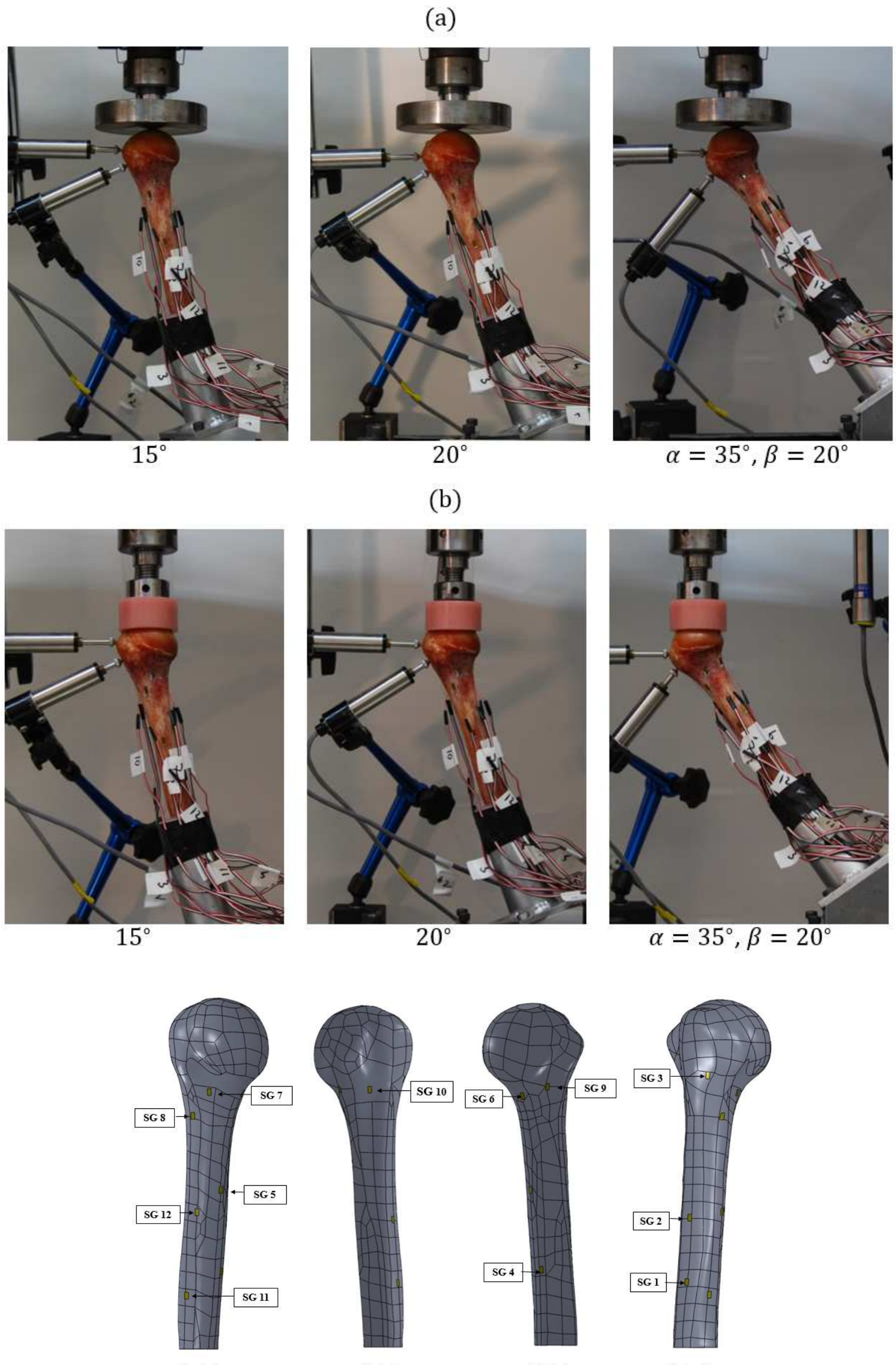

Figure 2: Top two figures: Experimental typical loadings using (a) a flat plate and (b) a conical shaped cup. Bottom: Left humerus showing typical SGs locations.

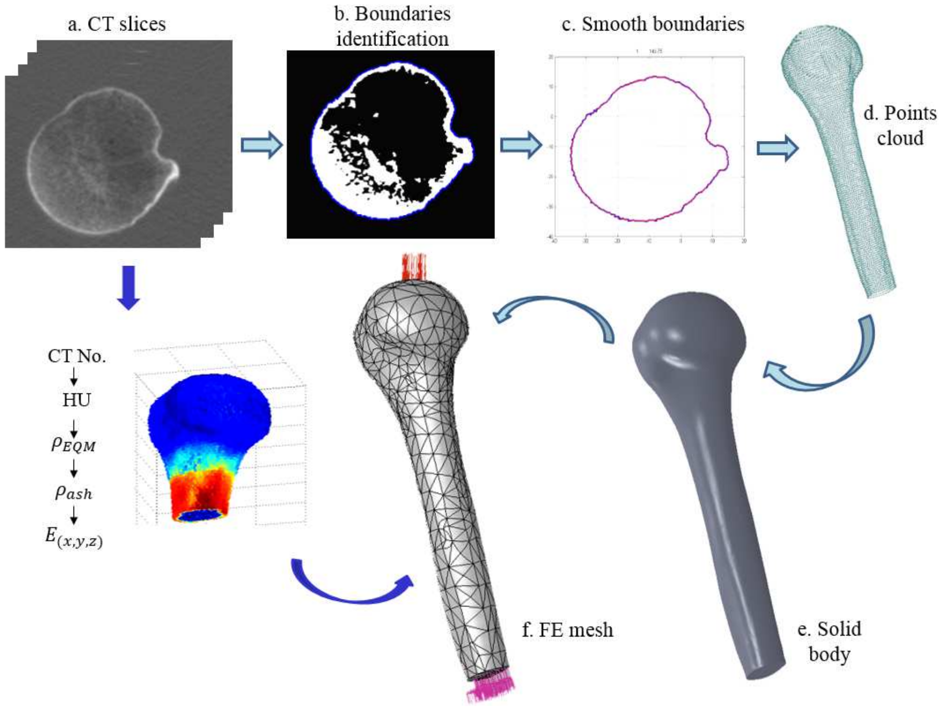

Figure 3: Schematic flowchart describing the generation of the FE model from QCT scans.

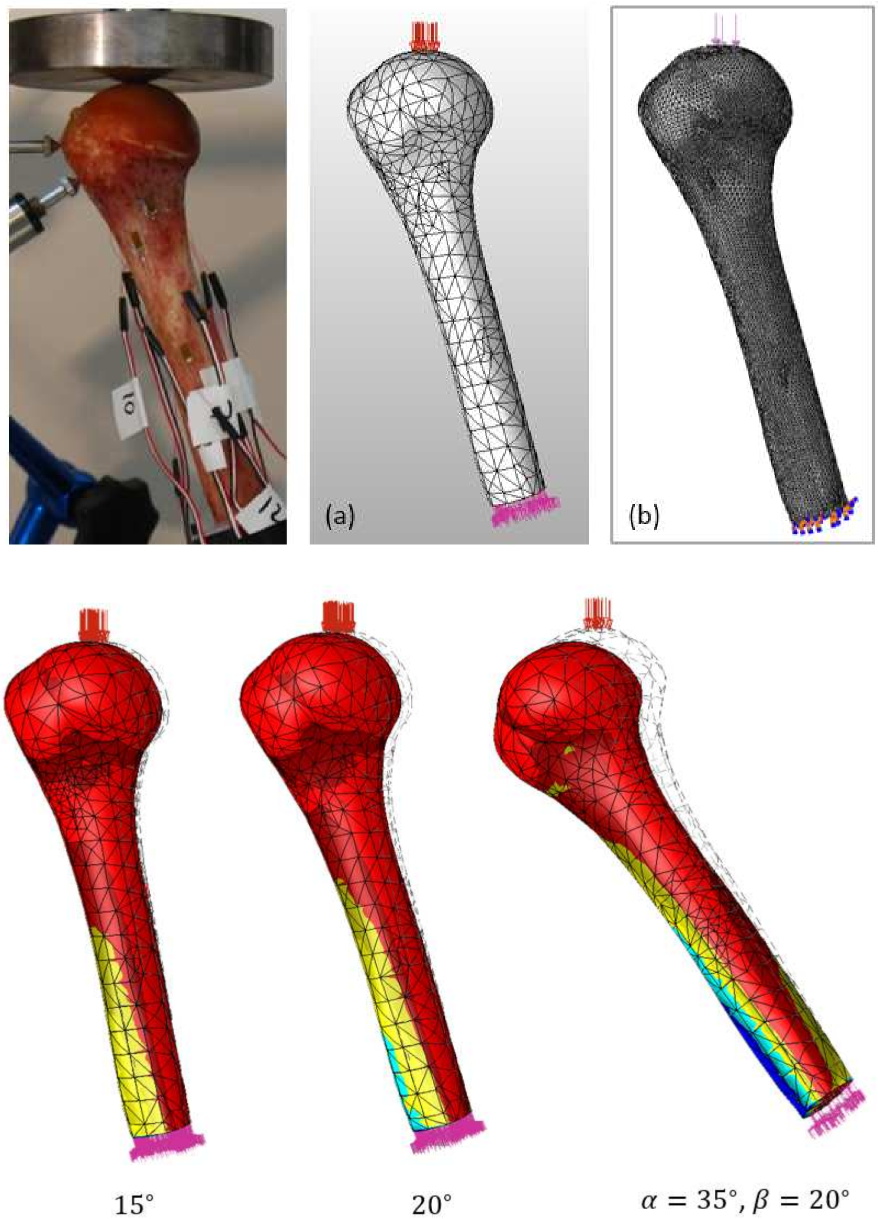

Figure 4: Top: FFH2L-20° flat plate loading- experiment, (a) p-FE model and (b) h-FE model. Bottom: Principal strain ϵ_3 at $800N$ computed by p-FEA for FFH2L.

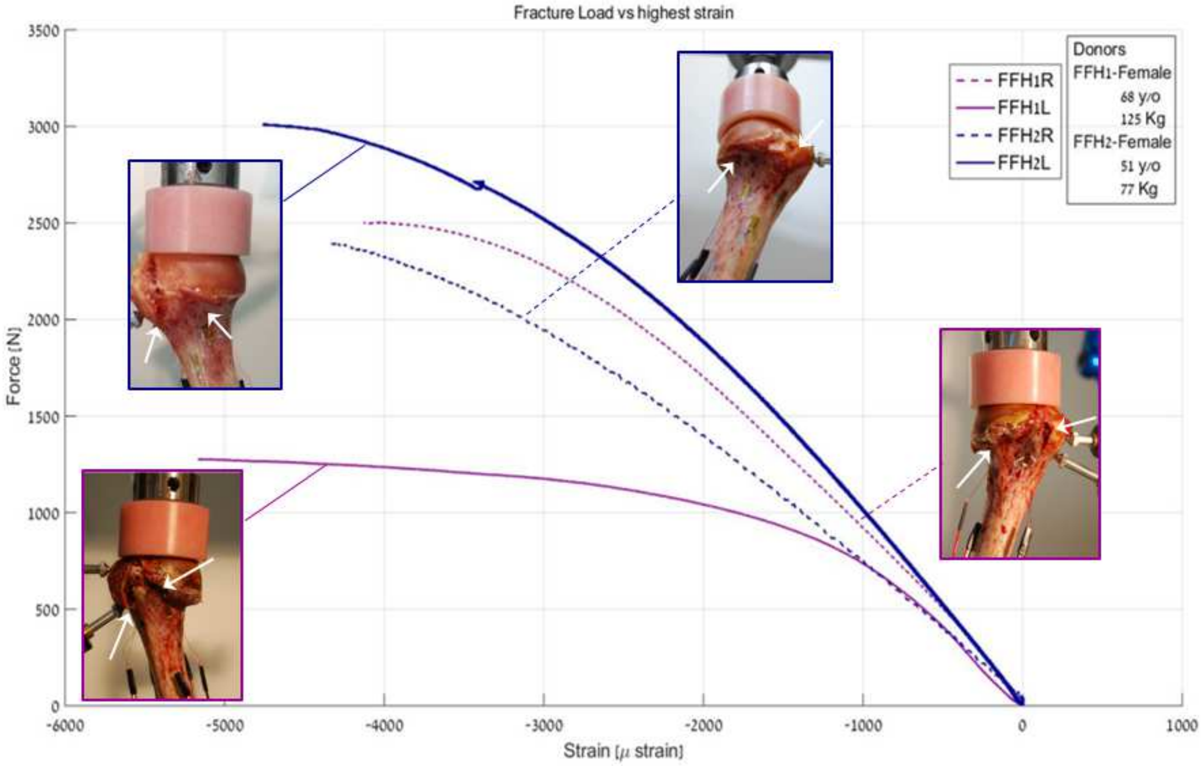

Figure 5: Load vs. largest measured strain in fracture experiments for FFH1 and FFH2, arrows indicate fracture locations.

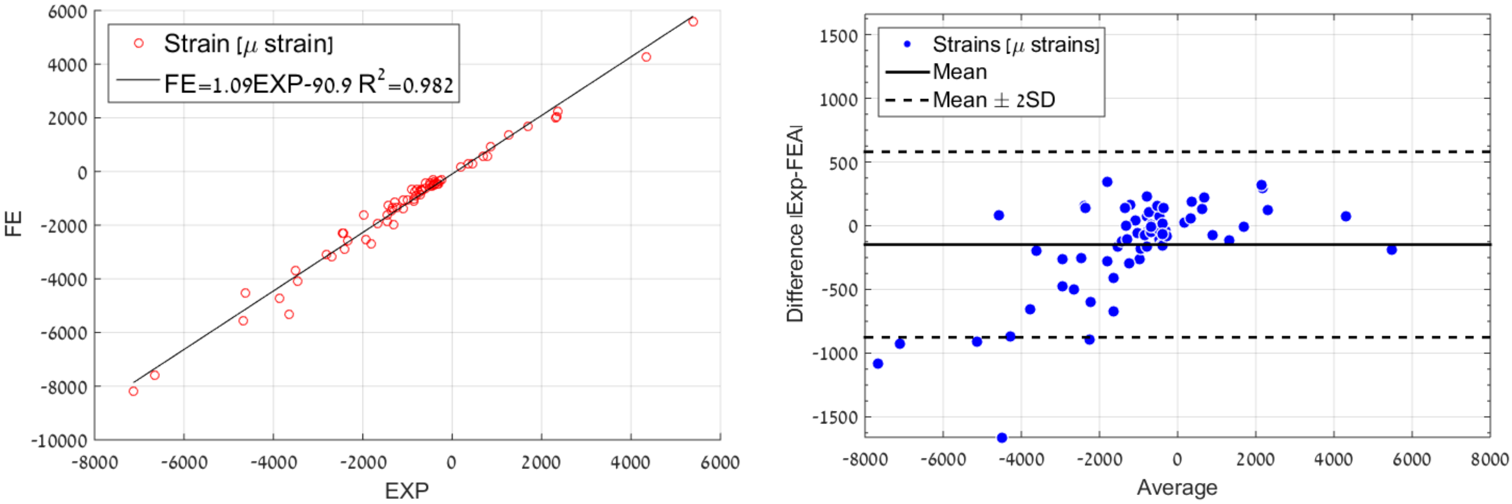

Figure 6: Linear correlation and Bland-Altman plots for FFH2 - Right and Left humeri at three inclination angles - flat plate load.

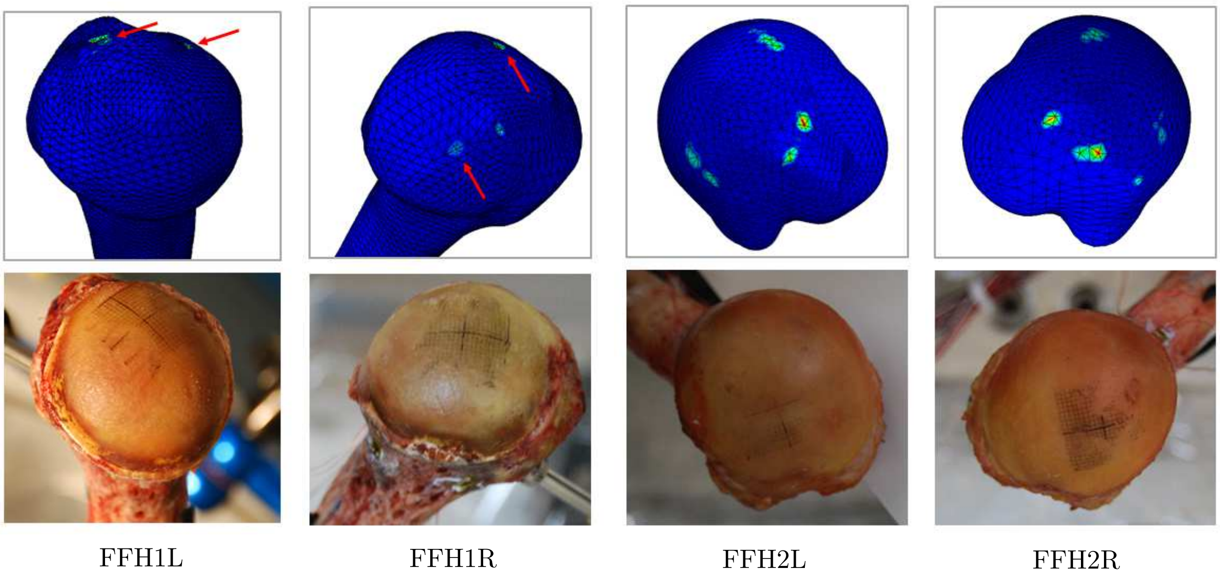

Figure 7: Contact area on humeri heads, as computed by contact analyses and observed in experiments (black marks on the humeri head).

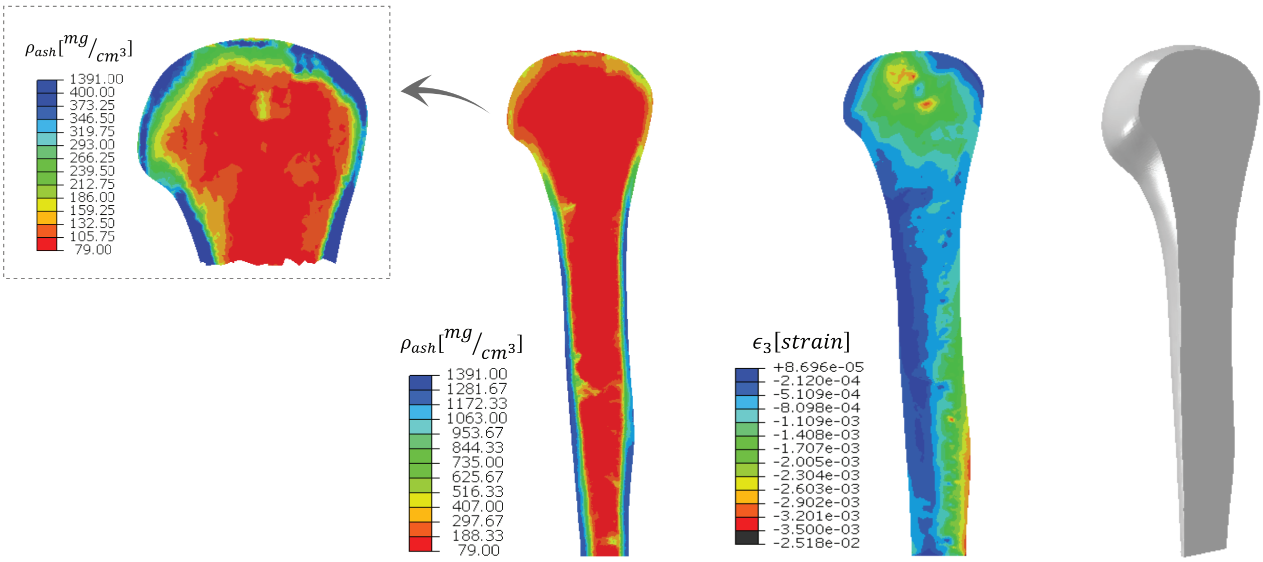

Figure 8: Ash density and predicted strains (minimum principal strains - ϵ_3) inside FFH2L.

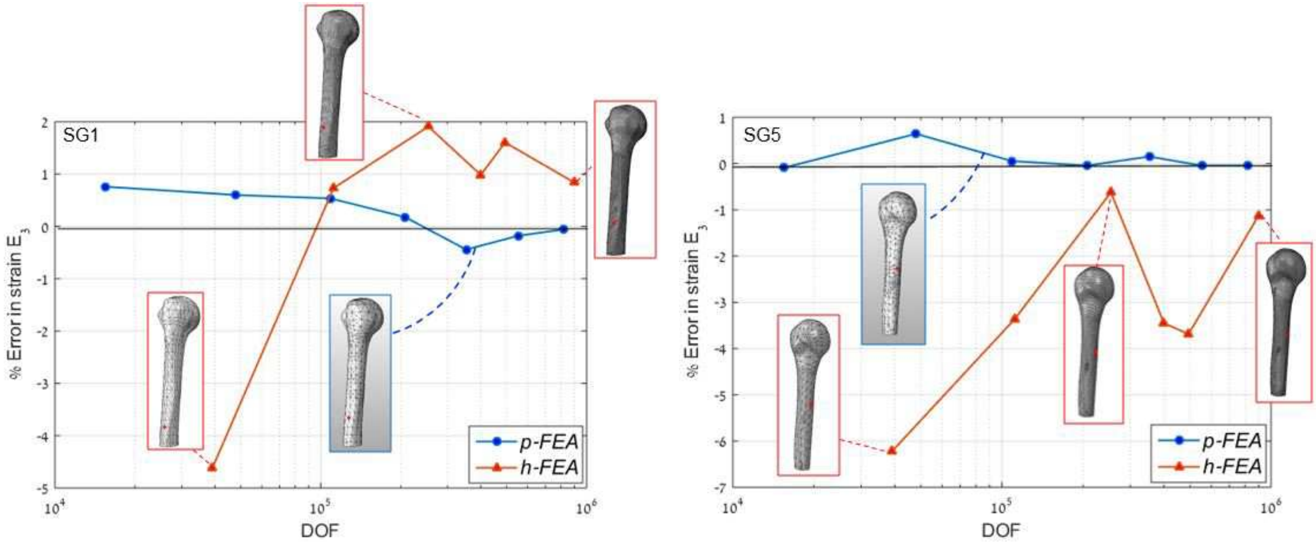

Figure 9: Convergence in strains, p-FE vs. Abaqus.